The end-to-end Calibration of LHAASO-WFCTA based on Nitrogen Laser System

Qinning Sun,[a,*] **Zhen Min,**[b,c] **Hu Liu,**[a] **Long Chen,**[a] **Yang Wang,**[a] **Fengrong Zhu**[a,†]
and Shoushan Zhang[b,c] **for the LHAASO collaboration**

[a]*Southwest Jiaotong University, School of Physical Science and Technology,*
No. 999, Xi'an Road, Chengdu, China

[b]*Institute of High Energy Physics, Chinese Academy of Sciences, Key Laboratory of Particle*
Astrophysics & Experimental Physics Division & Computing Center,
No. 19B Yuquan Road, Beijing, China

[c]*Institute of High Energy Physics, Chinese Academy of Sciences,TIANFU Cosmic Ray Research Center,*
No. 1500 Kezhi Road, Chengdu, China

E-mail: zhufr@home.swjtu.edu.cn

The Wide Field-of-view Cherenkov Telescope Array (WFCTA) of Large High Altitude Air Shower Observatory (LHAASO) is designed to perform nearly calorimetric measurements of extensive air showers induced by cosmic rays with energies between 10^{13} eV - 10^{18} eV. In order to achieve an end-to-end calibration of WFCTA and investigate properties of the atmospheric aerosol, five laser systems have been operated at LHAASO, including 3 nitrogen and 2 Nd:YAG laser devices. This work presents an overview of the laser signals received by the telescope and the monitoring of geometric information related to nitrogen laser events. Additionally, it introduces the simulation method for the LHAASO-WFCTA laser calibration system. Through prolonged and stable operation, a substantial amount of data has been accumulated, requiring further data analysis for the calibration of the telescope's absolute gain and measurement of aerosol extinction coefficients.

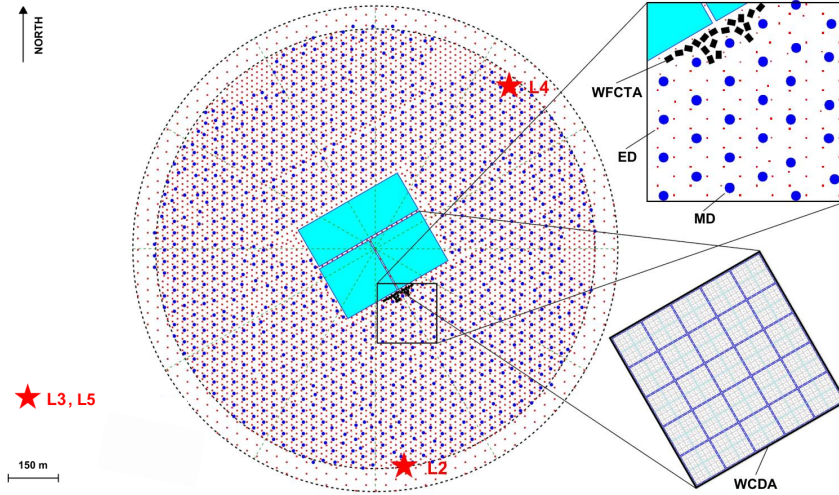[*]Speaker

1. Introduction

Figure 1: A LHAASO layout, positions of WFCTA, WCDA and KM2A are shown. Dashed lines indicate the outer edge of LHAASO and positions of laser facilities (L2, L3, L4, L5) are marked by red stars, L1 serving as a portable laser conducted experiments at various locations outside the base. L2, L4 and L5 utilized a nitrogen molecular laser, L1 and L3 employed a Nd:YAG laser.

The Large High Altitude Air Shower Observatory (LHAASO) [1, 2], locate in Haizishan National Natural Reserve with an altitude of 4410 *m* a.s.l., China. LHAASO consists of 3 major interconnected components, Kilometer Square array (KM2A) [3, 4], Water Cherenkov Detector Array (WCDA) [5] and the Wide Field of view Cherenkov Telescope Array (WFCTA) including 18 telescopes [1]. The main scientific goal of WFCTA is to probe cosmic ray spectra within the range of 10 TeV − 1 EeV together with WCDA and KM2A [6].

WFCTA observes primary cosmic rays by recording Cherenkov lights induced in extensive air shower. Photons are focused by spherical mirrors on the SiPM camera surface, where they are converted into electric pulses digitized by flash analogs-to-digital converters (FADCs). Atmospheric parameters have an impact on both production of Cherenkov photons and their attenuation towards WFCTA [7–11]. Thus, it is required to monitor the atmospheric quality and photon collection efficiency for WFCTA.

Laser calibration system of LHAASO consists of 3 nitrogen laser sites and 2 Nd:YAG laser sites [12–16]. Positions of laser sites in LHAASO is shown in Fig. 1. L1 is a mobile laser station that is dragged behind a carriage to search for fixed locations around the site. Its main purpose is to measure the local aerosol attenuation length and aerosol scattering phase function of LHAASO. On the other hand, L2-L5 are fixed stations within LHAASO, primarily used to measure the absolute gain of the telescopes and aerosol parameters.

This work discusses laser events collected by WFCTA in the second section and the laser simulation program in the third section.
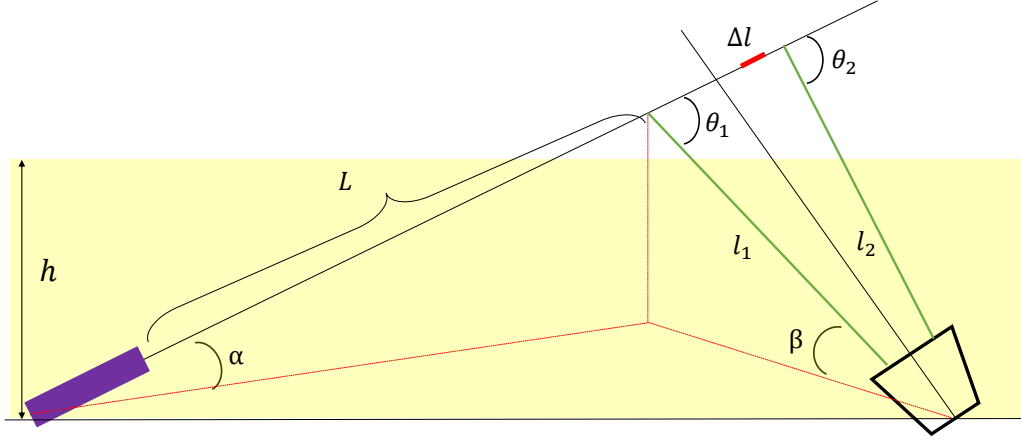
2. Laser signals received by the telescopes

Figure 2: The schematic diagram of laser emission shows a yellow shaded area of height *h*, which represents the region with significant aerosol impact. The purple line segment in the bottom left corner represents the laser emitter, and the trapezoid in the bottom right corner represents the telescope frame.

The process of laser propagation is shown in the Fig. 2. The intensity of the laser beam at a point is given by:

$$ADC = N \cdot \text{Gain} = N_0 \cdot e^{-(\tau_m + \tau_a)} \cdot (\Delta\tau_m \cdot P_m(\theta, \varphi) + \Delta\tau_a \cdot P_a(\theta, \varphi)) \cdot \Delta\Omega \cdot \text{Gain} \tag{1}$$

where ADC is total signal of element Δl on the scattering path, N is total photon arrived at telescope, $Gain$ indicates the collection efficient and the response of electronics, N_0 is number of photons per laser pulse, τ_m and τ_a are due to molecule and aerosol respectively, $\Delta\tau_m$ and $\Delta\tau_m$ is optical depth in Δl of air molecules and aerosol. $P_m(\theta, \varphi)$ and $P_a(\theta, \varphi)$ is phase function of Rayleigh and Mie scattering , $\Delta\Omega$ is solid angle of Δl towards telescope.

The laser is emitted at an elevation angle of α and propagates through distance of L in the atmosphere before entering the telescope field of view with a central elevation angle of β. After scattering at an angle of θ, the laser propagates a distance of l before entering the telescope.

During the data acquisition period of the WFCTA, the laser scans the field of view of the telescope at the specified angle. The propagation of laser beams through the atmosphere into the telescope's field of view involves interactions with air molecular and aerosol present in the atmosphere. As the laser beam interacts with these particles, scattering occurs, and the photons scattered in the direction towards the telescope are recorded. The telescopes are pointed at different azimuth angles with the same elevation angle. In order to calibrate all the telescopes and measure the vertical distribution of aerosol, the laser cruising scheme includes elevation ranging from 10° to 40°, with multiple azimuth angles for each elevation angle. Taking the L2 laser station for example, with an elevation angle of 30°, there are a total of 7 azimuth angles to cover all the telescope's field of view,

as shown in Fig. 3. Each azimuth angles continuely emitting laser for one minute with a frequency of 1 *Hz*.

The laser track in WFCTA is shown in Fig. 5 (a). In order to analyze geometric stability of laser
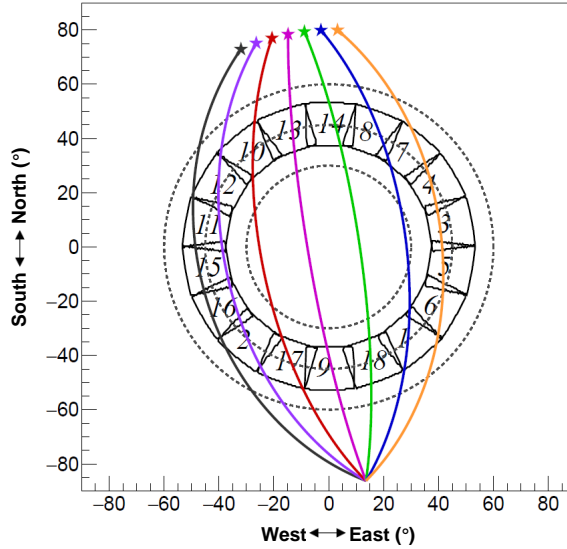

Figure 3: FOV of WFCTA and laser tracks pass through FOV of 18 telescopes outlined by the lines. The dashed arcs indicate zenith angles of 20°, 30°, and 40° from middle to edge, which covers 360° in azimuth. Different color lines indicate series of laser angle tracks with different laser emission azimuths at the zenith of 60° from L2. In the graph, the north direction is represented by an azimuth angle of 0°, and the positive direction is clockwise.

event, signals obtained are fitted with a straight line and calculate the slope and intercept of the line as shown in Fig. 5 (a). The geometry of laser events is related to the laser hardware and telescope direction, and the analysis of geometric data can be used to monitor the working status of the laser. The long-term geometric data of laser events is shown in the Fig. 4. The geometry of the laser events shown in the diagram correspond to the orange line in Fig. 3.

3. Simulation of calibration

The Monte Carlo simulation of laser consists of three parts: photon generation, propagation and detection [10].

The visual representation of laser event imaging generated by the Monte Carlo simulation method and experimental data imaging is illustrated in Fig. 5. Through the investigation of the simulation system, it has been found that the system can effectively replicate the experimental data and perform imaging. This indicates that the simulation system accurately models the real-world scenarios and provides reliable results in terms of data and imagery.

The photon generator includes simulations of laser spot size, spot divergence, polarization, photon number, pulse duration, wavelength and emission angle. The emission angle of the laser is
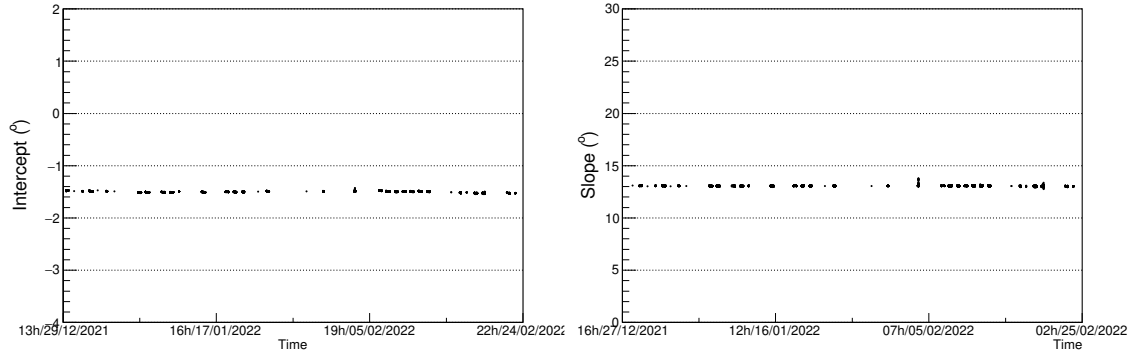
Figure 4: Long-term monitoring of the geometric information of laser events recorded by the telescope. The data presented in the figure is derived from the angle indicated by the orange line in Fig. 3, with an elevation angle of 30° and an azimuth angle of -64°.
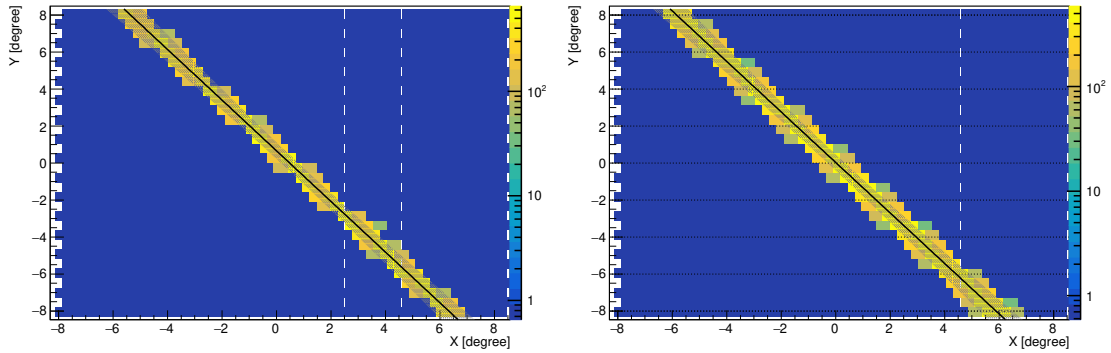

Figure 5: The images of the laser event for experimental data (left) and simulated data (right) of the same angle. This laser event originates from the L2 laser site, corresponding to the orange line at azimuth angle of -64° in Fig. 3. The experimental data is presented on the left side, while the simulated data is shown on the right side. The black line in the figure represents the fitting line of the image intensity.

changed by the high-precision 3D Lifting Rotating Platform (HiRoP) [17].

In the simulation of the photon propagation, the atmosphere is considered as two parts: air molecule and aerosol. The absorption and scattering of air molecule is described using the US Standard Atmosphere Model in the simulation. The scattering model for air molecules uses the Rayleigh scattering curve, while the scattering model for aerosols uses the Elbert model and the Longtin model under different wind speeds[18, 19]. Fig. 6 illustrates the Rayleigh scattering and the aerosol scattering phase functions of different models. The aerosol scattering phase functions have undergone normalization processing.

The telescope's detection simulation employs the same program as the cosmic ray simulation [20]. In Monte Carlo simulations, the geometric trajectory of the laser is well understood. Fig. 7 shows the differences in geometry between simulated and experimental data for various emission angles.
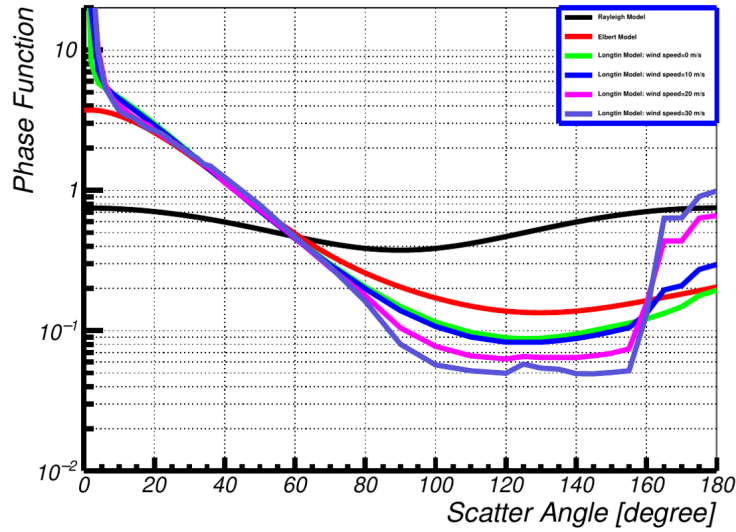
Figure 6: The scattering probability distribution as a function of scattering angle used in the simulation program is shown. The black line represents the probability distribution of Rayleigh scattering, while the red to blue lines represent the Mie scattering probability distributions for the Elbert model and the Longtin model at different wind speeds, respectively.

The discrepancy in intercepts between the imaging fits of experimental and simulated data is within ±0.3°, while the difference in slopes is within ±0.8°. This indicates that we can employ a set of turntable parameters to achieve directional reconstruction of all telescopes and laser emission angles within the required accuracy for the experiment.
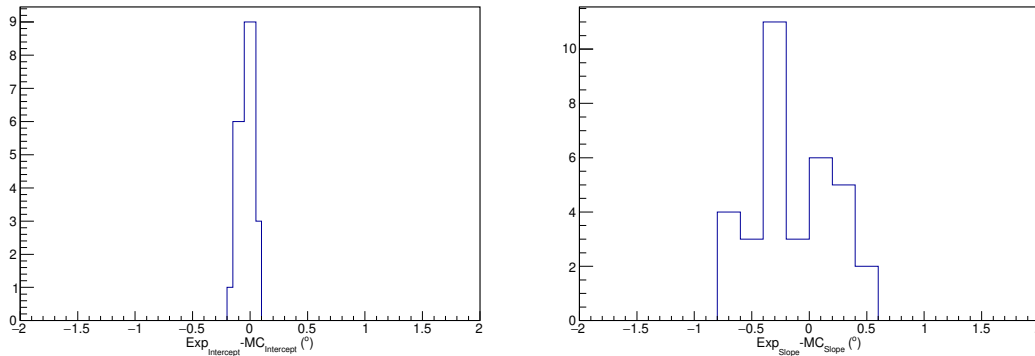

Figure 7: The figure displays the geometric difference between experimental and simulated data. The left panel shows the difference in intercepts, while the right panel shows the slopes.

To validate the accuracy of the Monte Carlo simulation, we have also developed a analytical method to calculate the propagation of laser beams. The analytical method employed allows for numerical calculations of the photon propagation process. It can provide preliminary validation of Monte Carlo simulation results concerning the overall generation, propagation, laser track geome-

try, and total photon number. However, this method does not encompass the simulation of internal characteristics within the telescope or the rendering of imaging.

After performing calculations, it has been observed that the total number of photons in the laser events generated through Monte Carlo simulations corresponds to the distribution of photons along the long axis of the laser events. These results align with the outcomes obtained through the analytical computational method. The analytical computational method can be employed for swift processing of laser events and for validating simulated results.

4. Summary and Prospects

After a prolonged period of operation, we have accumulated geometrically stable data and developed a simulation program to assist us in further refining the calibration of telescopes and aerosols. Geometric of laser event is well understood.

In the subsequent stages of our work, we will continue to advance in data and laser simulation analysis. To obtain calibration results for the absolute gain of the telescope and the aerosol extinction coefficient, we will first identify periods with preference clear nights, then analyze the variations in photon counts between these selected days and other days. By comparing the differences in photon counts, we can investigate the factors contributing to these variations.

Acknowledgement

References

[1] Z. Cao et al. Peta–electron volt gamma-ray emission from the Crab Nebula. *Science*, 373(6553):425–430, 2021.

[2] Z. Cao et al. Ultra high-energy photons up to 1.4 petaelectronvolts from 12 γ-ray galactic sources. *Nature*, 594(7861):33–36, 2021.

[3] Hong Kui Lv et al. Calibration of the LHAASO-KM2A electromagnetic particle detectors using charged particles within the extensive air showers. *Astroparticle Physics*, 100:22–28, 2018.

[4] F. Aharonian et al. Self-calibration of LHAASO-KM2A electromagnetic particle detectors using single particles within extensive air showers. *Phys. Rev. D*, 106:122004, Dec 2022.

[5] Xin Hua Ma et al. Chapter 1 LHAASO instruments and detector technology. *Chinese Physics C*, 46(3):030001, 2022.

[6] F. Aharonian et al. Reconstruction of cherenkov image by multiple telescopes of LHAASO-WFCTA. *Radiation Detection Technology and Methods*, 2022.

[7] F. Aharonian et al. Construction and on-site performance of the LHAASO WFCTA camera. *Eur. Phys. J. C*, 81:657, 2021.

[8] F. Aharonian et al. Absolute calibration of LHAASO WFCTA camera based on LED. *Nuclear Instruments and Methods in Physics Research Section A: Accelerators, Spectrometers, Detectors and Associated Equipment*, 1021:165824, 2022.

[9] Li.Qiao. Yin et al. The expectation of cosmic ray proton and helium energy spectrum below 4 PeV measured by LHAASO. *arXiv: High Energy Astrophysical Phenomena*, 2019.

[10] J. Abraham et al. A study of the effect of molecular and aerosol conditions in the atmosphere on air fluorescence measurements at the pierre auger observatory. *Astroparticle Physics*, 33(2):108–129, 2010.

[11] The Pierre Auger Collaboration. Techniques for measuring aerosol attenuation using the central laser facility at the pierre auger observatory. *Journal of Instrumentation*, 8(04):P04009, apr 2013.

[12] Qin. Ning. Sun et al. The YAG Lidar System Applied in LHAASO. *Proceedings of 37th International Cosmic Ray Conference*, 395:272, 2021.

[13] Long. Chen et al. Application of the nitrogen laser calibration system in LHAASO-WFCTA. *Proceedings of 37th International Cosmic Ray Conference*, 395:269, 2021.

[14] Ning. Xie et al. The Performance of the Laser Systems in the Calibration System of LHAASO-WFCTA. *Proceedings of 36th International Cosmic Ray Conference*, 358:498, 2019.

[15] Yang Wang et al. The Laser calibration system for LHAASO-WFCTA. *Proceedings of 37th International Cosmic Ray Conference*, 395:271, 2021.

[16] Sun Qinning et al. Design and development of laser temperature control system of lhaaso. *Journal of Instrumentation*, 18:T06008, 06 2023.

[17] X. Li et al. Experimental study on performance of a three-dimensional rotating and lifting platform in an imaging-lidar calibration system. *Astronomical Research & Technology*, 19(3):9, 2022.

[18] Wen Xuan Pi et al. Extinction coefficients of surface atmospheric aerosol above LHAASO. *Chinese Physics C*, 43(8):085001, aug 2019.

[19] Jun Ji Xia et al. Atmospheric depth models in the field of view of LHAASO-WFCTA. *Proceedings of 37th International Cosmic Ray Conference*, 395:244, 07 2021.

[20] Liping Wang et al. Cosmic ray mass independent energy reconstruction method using cherenkov light and muon content in LHAASO. *Phys. Rev. D*, 107:043036, Feb 2023.

Full Authors List: Collaboration

Zhen Cao[1,2,3], F. Aharonian[4,5], Q. An[6,7], Axikegu[8], L.X. Bai[9], Y.X. Bai[1,3], L.X. Bai[9], Y.X. Bai[1,3], Y.W. Bao[10], D. Bastieri[11], X.J. Bi[1,2,3], Y.J. Bi[1,3], H. Cai[12], J.T. Cai[11], Zhe Cao[6,7], J. Chang[13], J.F. Chang[1,3,6], B.M. Chen[14], E.S. Chen[1,2,3], J. Chen[9], Liang Chen[1,2,3], Liang Chen[15], Long Chen[8], M.J. Chen[1,3], M.L. Chen[1,3,6], Q.H. Chen[8], S.H. Chen[1,2,3], S.Z. Chen[1,3], T.L. Chen[16],X.L. Chen[1,2,3], Y. Chen[10], N. Cheng[1,3], Y.D. Cheng[1,3], S.W. Cui[14], X.H. Cui[17], Y.D. Cui[18], B. D'Ettorre Piazzoli[19], B.Z. Dai[20], H.L. Dai[1,3,6], Z.G. Dai[7], Danzengluobu[16], D. della Volpe[21], X.J. Dong[1,3], K.K. Duan[13], J.H. Fan[11], Y.Z. Fan[13], Z.X. Fan[1,3], J. Fang[20], K. Fang[1,3], C.F. Feng[22], L. Feng[13], S.H. Feng[1,3], Y.L. Feng[13], B. Gao[1,3], C.D. Gao[22], L.Q. Gao[1,2,3], Q. Gao[16], W. Gao[22], M.M. Ge[20], L.S. Geng[1,3], G.H. Gong[23], Q.B. Gou[1,3], M.H. Gu[1,3,6], F.L. Guo[15], J.G. Guo[1,2,3], X.L. Guo[8], Y.Q. Guo[1,3], Y.Y. Guo[1,2,3,13], Y.A. Han[24], H.H. He[1,2,3], H.N. He[13], J.C. He[1,2,3], S.L. He[11], X.B. He[18], Y. He[8], M. Heller[21], Y.K. Hor[18], C. Hou[1,3], H.B. Hu[1,2,3], S. Hu[9], S.C. Hu[1,2,3], X.J. Hu[23], D.H. Huang[8], Q.L. Huang[1,3], W.H. Huang[22], X.T. Huang[22], X.Y. Huang[13], Z.C. Huang[8], F. Ji[1,3], X.L. Ji[1,3,6], H.Y. Jia[8], K. Jiang[6,7], Z.J. Jiang[20], C. Jin[1,2,3], T. Ke[1,3], D. Kuleshov[25], K. Levochkin[25], B.B. Li[14], Cheng Li[6,7], Cong Li[1,3], F. Li[1,3,6], H.B. Li[1,3], H.C. Li[1,3], H.Y. Li[7,13], J. Li[1,3,6], K. Li[1,3], W.L. Li[22], X.R. Li[1,3], Xin Li[6,7], Xin Li[8], Y. Li[9], Y.Z. Li[1,2,3], Zhe Li[1,3], Zhuo Li[26], E.W. Liang[27], Y.F. Liang[27], S.J. Lin[18], B. Liu[7], C. Liu[1,3], D. Liu[22], H. Liu[8], H.D. Liu[24], J. Liu[1,3], J.L. Liu[28], J.S. Liu[18], J.Y. Liu[1,3], M.Y. Liu[16], R.Y. Liu[10], S.M. Liu[8], W. Liu[1,3], Y. Liu[11], Y.N. Liu[23], Z.X. Liu[9], W.J. Long[8], R. Lu[20], H.K. Lv[1,3], B.Q. Ma[26], L.L. Ma[1,3], X.H. Ma[1,3], J.R. Mao[29], A. Masood[8], Z. Min[1,3], W. Mitthumsiri[30], T. Montaruli[21], Y.C. Nan[22], B.Y. Pang[8], P. Pattarakijwanich[30], Z.Y. Pei[11], M.Y. Qi[1,3], Y.Q. Qi[14], B.Q. Qiao[1,3], J.J. Qin[7], D. Ruffolo[30], V. Rulev[25], A. Sáiz[30], L. Shao[14], O. Shchegolev[25,31], X.D. Sheng[1,3], J.Y. Shi[1,3], H.C. Song[26], Yu.V. Stenkin[25,31], V. Stepanov[25], Y. Su[32], Q.N. Sun[8], X.N. Sun[27], Z.B. Sun[33], P.H.T. Tam[18], Z.B. Tang[6,7], W.W. Tian[2,17], B.D. Wang[1,3], C. Wang[33], H. Wang[8], H.G. Wang[11], J.C. Wang[29], J.S. Wang[28], L.P. Wang[22], L.Y. Wang[1,3], R.N. Wang[8], W. Wang[18], W. Wang[12], X.G. Wang[27], X.J. Wang[1,3], X.Y. Wang[10], Y. Wang[8], Y.D. Wang[1,3], Y.J. Wang[1,3], Y.P. Wang[1,2,3], Z.H. Wang[9], Z.X. Wang[20], Zhen Wang[28], Zheng Wang[1,3,6], D.M. Wei[13], J.J. Wei[13], Y.J. Wei[1,2,3], T. Wen[20], C.Y. Wu[1,3], H.R. Wu[1,3], S. Wu[1,3], W.X. Wu[8], X.F. Wu[13], S.Q. Xi[1,3], J. Xia[7,13], J.J. Xia[8], G.M. Xiang[2,15], D.X. Xiao[16], G. Xiao[1,3], H.B. Xiao[11], G.G. Xin[12], Y.L. Xin[8], Y. Xing[15], D.L. Xu[28], R.X. Xu[26], L. Xue[22], D.H. Yan[29], J.Z. Yan[13], C.W. Yang[9], F.F. Yang[1,3,6], J.Y. Yang[18], L.L. Yang[18], M.J. Yang[1,3], R.Z. Yang[7], S.B. Yang[20], Y.H. Yao[9], Z.G. Yao[1,3], Y.M. Ye[23], L.Q. Yin[1,3], N. Yin[22], X.H. You[1,3], Z.Y. You[1,2,3], Y.H. Yu[22], Q. Yuan[13], H.D. Zeng[13], T.X. Zeng[1,3,6], W. Zeng[20], Z.K. Zeng[1,2,3], M. Zha[1,3], X.X. Zhai[1,3], B.B. Zhang[10], H.M. Zhang[10], H.Y. Zhang[22], J.L. Zhang[17], J.W. Zhang[9], L.X. Zhang[11], Li Zhang[20], Lu Zhang[14], P.F. Zhang[20], P.P. Zhang[14], R. Zhang[7,13], S.R. Zhang[14], S.S. Zhang[1,3], X. Zhang[10], X.P. Zhang[1,3], Y.F. Zhang[8], Y.L. Zhang[1,3], Yi Zhang[1,13], Yong Zhang[1,3], B. Zhao[8], J. Zhao[1,3], L. Zhao[6,7], L.Z. Zhao[14], S.P. Zhao[13,22], F. Zheng[33], Y. Zheng[8], B. Zhou[1,3], H. Zhou[28], J.N. Zhou[15], P. Zhou[10], R. Zhou[9], X.X. Zhou[8], C.G. Zhu[22], F.R. Zhu[8], H. Zhu[17], K.J. Zhu[1,2,3,6] and X. Zuo[1,3]

[1]Key Laboratory of Particle Astrophyics & Experimental Physics Division & Computing Center, Institute of High Energy Physics, Chinese Academy of Sciences, 100049 Beijing, China.

[2]University of Chinese Academy of Sciences, 100049 Beijing, China.

[3]TIANFU Cosmic Ray Research Center, Chengdu, Sichuan, China.

[4]Dublin Institute for Advanced Studies, 31 Fitzwilliam Place, 2 Dublin, Ireland.

[5]Max-Planck-Institut for Nuclear Physics, P.O. Box 103980, 69029 Heidelberg, Germany.

[6]State Key Laboratory of Particle Detection and Electronics, China.

[7]University of Science and Technology of China, 230026 Hefei, Anhui, China.

[8]School of Physical Science and Technology & School of Information Science and Technology, Southwest Jiaotong University, 610031 Chengdu, Sichuan, China.

[9]College of Physics, Sichuan University, 610065 Chengdu, Sichuan, China.

[10]School of Astronomy and Space Science, Nanjing University, 210023 Nanjing, Jiangsu, China.

[11]Center for Astrophysics, Guangzhou University, 510006 Guangzhou, Guangdong, China.

[12]School of Physics and Technology, Wuhan University, 430072 Wuhan, Hubei, China.

[13]Key Laboratory of Dark Matter and Space Astronomy, Purple Mountain Observatory, Chinese Academy of Sciences, 210023 Nanjing, Jiangsu, China.

[14]Hebei Normal University, 050024 Shijiazhuang, Hebei, China.

[15]Key Laboratory for Research in Galaxies and Cosmology, Shanghai Astronomical Observatory, Chinese Academy of Sciences, 200030 Shanghai, China.

[16]Key Laboratory of Cosmic Rays (Tibet University), Ministry of Education, 850000 Lhasa, Tibet, China.

[17]National Astronomical Observatories, Chinese Academy of Sciences, 100101 Beijing, China.

[18]School of Physics and Astronomy & School of Physics (Guangzhou), Sun Yat-sen University, 519000 Zhuhai, Guangdong, China.

[19]Dipartimento di Fisica dell'Università di Napoli `Federico II", Complesso Universitario di Monte Sant'Angelo, via Cinthia, 80126 Napoli, Italy.

[20]School of Physics and Astronomy, Yunnan University, 650091 Kunming, Yunnan, China.

[21]D'epartement de Physique Nucl'eaire et Corpusculaire, Facult'e de Sciences, Universit'e de Gen'eve, 24 Quai Ernest Ansermet, 1211 Geneva, Switzerland.

PoS(ICRC2023)494

[22] Institute of Frontier and Interdisciplinary Science, Shandong University, 266237 Qingdao, Shandong, China.

[23] Department of Engineering Physics, Tsinghua University, 100084 Beijing, China.

[24] School of Physics and Microelectronics, Zhengzhou University, 450001 Zhengzhou, Henan, China.

[25] Institute for Nuclear Research of Russian Academy of Sciences, 117312 Moscow, Russia.

[26] School of Physics, Peking University, 100871 Beijing, China.

[27] School of Physical Science and Technology, Guangxi University, 530004 Nanning, Guangxi, China.

[28] Tsung-Dao Lee Institute & School of Physics and Astronomy, Shanghai Jiao Tong University, 200240 Shanghai, China.

[29] Yunnan Observatories, Chinese Academy of Sciences, 650216 Kunming, Yunnan, China.

[30] Department of Physics, Faculty of Science, Mahidol University, 10400 Bangkok, Thailand.

[31] Moscow Institute of Physics and Technology, 141700 Moscow, Russia.

[32] Key Laboratory of Radio Astronomy, Purple Mountain Observatory, Chinese Academy of Sciences, 210023 Nanjing, Jiangsu, China.

[33] National Space Science Center, Chinese Academy of Sciences, 100190 Beijing, China.